Carbohydrate Polymers 87 (2012) 799–805

Contents lists available at SciVerse ScienceDirect

Carbohydrate Polymers

journal homepage: www.elsevier.com/locate/carbpol

Outstanding reinforcing effect of highly oriented chitin whiskers in PVA nanocomposites

Ahmed Jalal Uddin, Masahiro Fujie, Shinichiro Sembo, Yasuo Gotoh*

Faculty of Textile Science and Technology, Shinshu University, 3-15-1 Tokida, Ueda, Nagano 386-8567, Japan

ARTICLE INFO

Article history:
Received 12 June 2011
Accepted 23 August 2011
Available online 31 August 2011

Keywords:
Nanocomposites
Chitin whiskers
Poly(vinyl alcohol)
Interfacial interaction
Mechanical properties
Creep

ABSTRACT

To utilize the extreme reinforcing performance of chitin whiskers (ChWs), the current work was undertaken to fabricate nanocomposites embedded with highly uniaxial oriented ChWs into the matrix polymer. Fibers of poly(vinyl alcohol) (PVA)/ChWs were prepared by gel spinning and the fibers were subjected to a hot drawing to their maximal draw ratio. WAXD analysis revealed the very high orientation of ChWs in the PVA matrix. DSC measurements showed that, upon ChWs loadings, crystallinity of PVA increased and non-isothermal cooling crystallization peak of PVA shifted towards lower temperature, indicating the interaction of PVA with ChWs. Measurement of infrared dichroism suggested that the orientation of overall PVA chains increased with the increase in ChWs loading due to the possible dragging of PVA chains attached with ChWs during drawing, which resulted higher PVA crystallinity in the composites. The stress transfer in PVA/ChWs interface quantified by X-ray diffraction evidenced the strong adherence between the two. The stress transfer between PVA and ChWs interface, and higher PVA crystallinity induced by ChWs were reflected to the outstanding enhancement in mechanical- and anti-creep properties of nanocomposite fibers.

1. Introduction

Recent interest in solid waste management and biodegradable products has led to a policy of developing environment-friendly materials. Significant attention has been devoted in the past two decades to fabricate polymer nanocomposites, in which incorporation of mechanically robust, high aspect ratio nanoscale fillers markedly enhanced thermomechanical properties compared to the neat polymer or conventional composites (Hussain, Hojjati, Okamoto, & Gorga, 2006). As nanofillers, cellulose whiskers have attracted particular interest in academia and industry, because of their outstanding mechanical properties, natural abundance and renewable nature (Azizi Samir, Alloin, & Dufresne, 2005; Habibi, Lucia, & Rojas, 2010). Chitin, a structural polymer found in the outer skeleton of insects, crabs, shrimps, and lobsters, and in the internal structures of other invertebrates, is, after cellulose, the second most abundant natural polymer. Chitin is recognized as a biocompatible material because of its low antigenicity, low toxicity and biodegradability. Several research studies have reported its uses in medicine, e.g. absorbable sutures, drug carriers, and veterinary applications (Kumar, Muzzareli, Muzzareli, Sashiwa, & Domb, 2004).

The incorporation of chitin whiskers (ChWs) as reinforcing nanofillers in polymer matrices has broadened the utilization of chitin in preparation of a new class of biocomposite material. The mechanical performance of nanocomposites is highly influenced by the inherent properties of the nanofiller and the matrix itself, and the interactions and stress transfer at the filler/matrix interface (Wang, Ciselli, & Peijs, 2007). Since high aspect ratio nanofillers can exert their extreme performance along the length, thus uniaxial orientation of nanofillers in composites is highly desirable. The stress transfer from matrix to filler was found to greatly promote with the orientation of the filler (Rusli, Shanmuganathan, Rowan, Weder, & Eichhorn, 2010). An effective way to orient nanofillers in composites is to prepare nanocomposite fibers with high draw ratio.

Poly(vinyl alcohol) (PVA), a water-soluble and biodegradable polymer, is compatible with ChWs and several attempts were taken to fabricate PVA/α-chitin whisker composite films or electrospun nanofibers (Junkansem, Rujiranavit, & Supaphol, 2006; Junkansem, Rujiranavit, Grady, & Supaphol, 2010; Kadokawa, Takegawa, Mine, & Prasad, 2011; Sriuayo, Supaphol, Blackwell, & Rujiranavit, 2005). Other than films or nanofibers, highly drawn PVA fiber has some unique applications. For example, high-strength and high-modulus PVA fiber is being used as fiber reinforced cementitious (FRC) materials to not only reduce the weight of structural materials, but also to improve their ductility, toughness, and crack resistance (Sun, Chen, Luo, & Qian, 2001). As a low density and relatively inexpensive reinforcement for concrete, the demand of PVA is increasing to replace asbestos, steel and glass fibers (Zheng & Feldman, 1995). Moreover, the surface hydroxy groups of PVA fiber are known to

* Corresponding author. Tel.: +81 268 21 5366; fax: +81 268 25 9212.
E-mail address: ygotohy@shinshu-u.ac.jp (Y. Gotoh).

0144-8617/$ – see front matter © 2011 Elsevier Ltd. All rights reserved.
doi:10.1016/j.carbpol.2011.08.071

be easily attached to latex to form a rubber composite, and hence PVA fibers are used in the rubber industry to reinforce rubber hoses, conveyer belts and tire cords (Eichhorn, Hearle, Jaffe, & Mikutani, 2009). The increase in the performance of PVA fiber is expected to widen its utilization in those applications.

The present work was undertaken to enhance the performance of PVA fiber by incorporating highly uniaxial oriented ChWs into its matrix. The PVA/ChWs aqueous suspensions were extruded into cold methanol to obtain gel fibers and the produced fibers were drawn to the maximum extent, called maximal draw ratio (DR_{max}) (Uddin et al., 2006). The interaction and the stress transfer mechanism between matrix and filler, the prime determining factors to assess the performance of nanocomposites, were explored first and then the mechanical properties of the nanocomposite fibers were investigated.

2. Experimental

2.1. Matrix polymer

PVA chips (Poval-HC, Kuraray Co. Ltd., Japan) with a degree of polymerization (DP) of ca. 1500 and saponification of 99.9% were used.

2.2. Chitin whiskers (ChWs)

The chitin whiskers were prepared according to the previously reported method (Junkansem et al., 2010). Briefly, chitin flakes from crab shells (Tokyo chemical industry Co. Ltd.) were hydrolyzed with 3 N HCl at boil for 6 h under vigorous stirring. The suspension was then diluted with distilled water followed by centrifugation and dialysis. The concentration of the final whisker suspension was 6.5 wt%. From a number of transmission electron microscope (TEM) images, the length and diameters of ChWs were measured to be 100–500 nm and 10–50 nm, respectively, with an average aspect ratio of 15. Such a wide range in lengths and widths of ChWs with similar aspect ratio was reported before for the crab shell derived chitin whiskers (Nair & Dufresne, 2003).

2.3. Preparation of PVA–ChW suspensions

PVA chips were dissolved in distilled water in a static rotary mixer (50 rpm) at 80 °C for 2 h to obtain a 30 wt% PVA solution. A varying amounts of as-prepared 6.5 wt% whisker suspension and water were added (or evaporated) to the PVA solution to adjust the PVA concentration to 15% and the ChW concentration to 3, 5, 10, 15, 20 and 30% (of the weight of the solid PVA content). All the mixtures were homogenized in the rotary mixer at 80 °C for 1 h and then at 90 °C for 30 min. A separate spinning dope containing only 15 wt% PVA was also prepared for making neat PVA fibers for comparison.

2.4. Gel spinning and hot drawing

Gel spinning was carried out using a syringe pump and a syringe with a needle. The heater surrounding the syringe was set to 75 °C, and the spinning dopes were injected at 0.38 ml min^{-1} through a 0.80-mm diameter, 55-mm long needle into cooled methanol maintaining the temperature at −20 °C. After a 2-day drying in air, the fibers were drawn in a hot oven at 210 °C to their DR_{max}.

2.5. Characterization of samples

Wide-angle X-ray diffraction (WAXD) was carried out with a Rigaku Rotorflex RU200B X-ray generator operated at 40 kV and 150 mA. The radiation was Ni-filtered Cu-K_α (wavelength 0.15418 nm). The degree of crystal orientation (f_c) of PVA in the composites was determined from $f_c = (180 - H^0)/180$ (Nishino, Matsui, & Nakamae, 1999), where H^0 is the half-width of the intensity distribution curve along the Debye–Scherrer ring.

Differential scanning calorimetry (DSC) analyses were performed with a Rigaku ThermoPlus II. The measurements were carried out at heating rate of 10 °C min^{-1} in a dry nitrogen atmosphere. The degree of crystallinity (χ_c) of the PVA component in composite fibers was calculated from $\chi_c = \Delta H_m/w\Delta H_m{}^0$ where $\Delta H_m{}^0 = 161$ J g^{-1} is the heat of fusion for 100% crystalline PVA (Kubo & Kadla, 2003), ΔH_m is the heat of fusion and w is the weight fraction of the PVA in composites.

Using an FTIR-8400S instrument (Shimadzu Ltd., Japan) the orientation function of PVA component was determined by infrared dichroism, employing the –CH stretching vibration at 2930 cm^{-1} (Holland & Hay, 2001) according to the formula,

$$f = \frac{(D-1)(D_0+2)}{(D+2)(D_0-1)}$$

where D_0 is the dichroic ratio for perfectly oriented material, and is related to the transition moment direction (α) by the expression: $D_0 = 2\cot^2\alpha$. Here $\alpha = 90^\circ$ is used. The dichroic ratio (D) is defined by, $D = A_{||}/A_\perp$ where $A_{||}$ and $A_\perp$ represent the peak absorbances of infrared radiation polarized parallel and perpendicular to the orientation direction after subtracting the baseline intensity. Details of the measurement method are given in previous articles (Estes, Seymour, & Cooper, 1971; Read & Stein, 1968).

Tensile properties were measured at room temperature with a Shimadzu EZ-S instrument, using a 50 N load cell, 20 mm gauge length and 20 mm min^{-1} crosshead speed. The experimental results were evaluated as averages of at least 10 measurements.

The morphology of the fibers was examined using a Hitachi S-2380 N scanning electron microscope (SEM) with accelerating voltage 25 kV after sputter coating the samples with platinum.

Dynamic mechanical analysis (DMA) was performed in tensile mode using an ITK Co. DVA-225 instrument, at frequency 10 Hz, strain amplitude 0.15% and heating rate 10 °C min^{-1} on fibers of 20 mm in length.

Creep strain under constant load was measured using a Rigaku Denki model CN-8361 instrument. A single fiber 5 mm in length was subjected to a constant stress (300 MPa) at 120 °C, and the time-dependent strain was recorded for 6 h.

2.5.1. Measurement of stress transfer

For the fiber reinforced microcomposites, several test methods such as fiber pull-out, microbond test and push-in test were developed for measuring fiber–matrix adhesion using single fibers (Quan, Li, Yang, & Huang, 2005). When the fillers have nanoscale dimensions those methods are not applicable. In this context, we employed X-ray diffraction as a reliable technique to investigate the nanofiller–matrix interaction in composites (Uddin, Araki, & Gotoh, 2011).

Fig. 1 shows the meridional X-ray diffraction profile of PVA–ChW 30% fibers where distinct reflections of chitin- and PVA crystals are observed. To study the stress-transfer mechanism, a bundle of straight and parallel fibers were clamped in a stretching device attached to a load cell (Sakurada, Nukushima, & Ito, 1962). The whole set-up was placed in the X-ray goniometer. Constant stress (σ) was applied to the fibers in a direction parallel to the fiber axis. The effective stress (σ_c) on the ChWs in the composite was determined from the strain in the crystal lattice from the peak shift of the meridional (0 0 2) and (0 0 4) reflections of chitin crystals. The diffraction angle (2θ) was converted into lattice spacing 'd' using Bragg's equation, $\lambda = 2d\sin\theta$, where λ is the wavelength of the X-rays. The strain ε_c in the chitin crystals was estimated using the relationship, $\varepsilon_c = \Delta d/d_0$, where d_0 denotes the initial lattice spacing, and Δd is the change in lattice spacing induced by a

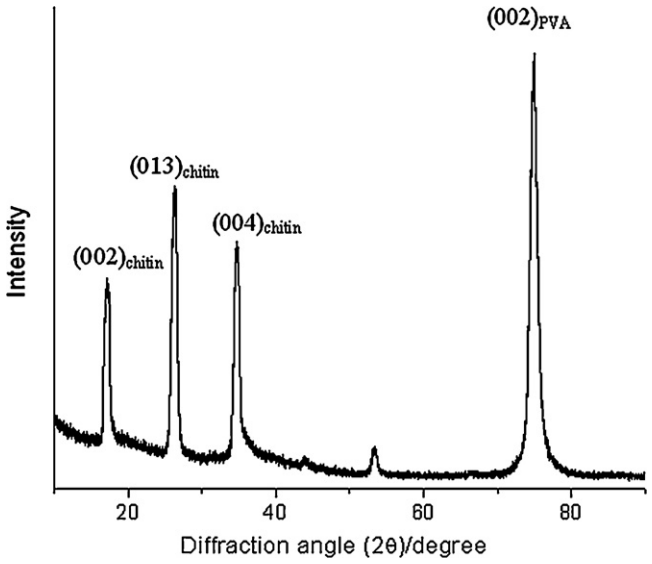

Fig. 1. Meridional X-ray diffraction profile of PVA–ChW 30% fibers.

constant stress. The effective stress (σ_c) on the incorporated ChWs was calculated from, $\sigma_c = \varepsilon_c \times E_l$, where E_l is the elastic modulus of the crystalline regions of chitin in the direction parallel to the chain axis (41 GPa) (Nishino et al., 1999).

3. Results and discussion

3.1. Interfacial interaction between ChWs and PVA

The WAXD patterns of the neat PVA and PVA-CW 30% fibers are shown in Fig. 2. The fibers exhibited diffractions from both highly oriented ChWs and PVA crystallites. Some sharp diffraction spots of the α-chitin crystals were indexed as (0 1 3), (0 0 2), (0 2 0) and (1 1 0/1 2 0) (overlapped with the 1 0 1/1 0 $\bar{1}$ plane of PVA) (Minke & Blackwell, 1978). Table 1 lists the DR_{max}, fiber diameters and thermal properties (heat of fusion, ΔH_m, crystallinity, χ_c, and melting temperature, T_m) of the PVA obtained by DSC. An interesting trend here is that χ_c gradually increased with ChW loading in the composites though DR_{max} decreased for highly ChW loaded fibers due to the increase in fiber stiffness. Fig. 3(left *Y*-axis) shows the calculated degree of crystal orientation (f_c) of PVA, determined from the (2 0 0) plane by X-ray diffraction. Fig. 3(right *Y*-axis) also shows the orientation function of the –CH component (f) of PVA, implying overall chain orientation of PVA, determined from infrared dichroism. Upon ChWs loading, the f_c was almost constant but f tended increasing towards negative indicating the increase in overall chain orientation of PVA along the fiber axis that places –CH bonds of PVA perpendicular to the chain. It should be noted here that in case of a full orientation of PVA chains along the fiber axis, i.e., fully perpendicular arrangement of –CH bonds with respect to the fiber axis, the f value can be maximum −0.5 (Read & Stein, 1968). However, though DR_{max} decreased with increasing ChW loading in composites, the increase in f value can be assumed to be generated from the possible dragging of PVA chains adhered with ChWs while ChWs were oriented along the fiber axis during drawing process. As seen in Table 1, the increase in χ_c in the composites with the increase in ChW content can be thought to be the result of the ChWs-induced PVA chains orientation. The substantial increase in χ_c in composites is reflected to the higher T_m values.

Fig. 4 shows DSC thermograms of dynamic cooling crystallization of the nanocomposite fibers. The crystallization temperature (T_c) of PVA gradually shifted towards lower temperature with increasing ChW content. This phenomenon substantiated the interaction between PVA and ChWs, where PVA chains adhered with the ChWs surface were likely to inhibit crystal growth by restricting the mobility of surrounding PVA chains.

Fig. 5 illustrates the temperature dependence of dynamic tan δ curves of the neat PVA and nanocomposite fibers. The α-relaxation peak of neat PVA at around 50 °C, associated to the glass transition (T_g), shifts to higher temperature and decreases in height with increasing ChW loading in composites. With the increase in ChWs loading, the α-relaxation peak changes its profile and shifts towards higher temperature may result from the two possible facts. The first one is due to likely for the interaction of PVA molecules with the surface of ChWs. This coupling effect may result in a restricted molecular mobility of PVA chains in contact with the ChWs surface. Higher matrix/filler adhesion was reported to give the broader tan δ peak in fiber–filled composites (Nielsen & Landel, 1994). The second reason could be the increased PVA crystallinity ascribed to the presence of ChWs (Table 1). However, the two mentioned reasons could be involved simultaneously in the observed change in the profile and shift of tan δ peaks.

3.2. Stress transfer between PVA and ChWs

Fig. 6 shows the relationship between the stress applied to the composite fibers (σ) and the effective stress (σ_c) on the ChWs. The σ_c is nearly 2-fold larger than the σ, indicating that the stress applied to the samples was greatly transferred to the filler ChWs

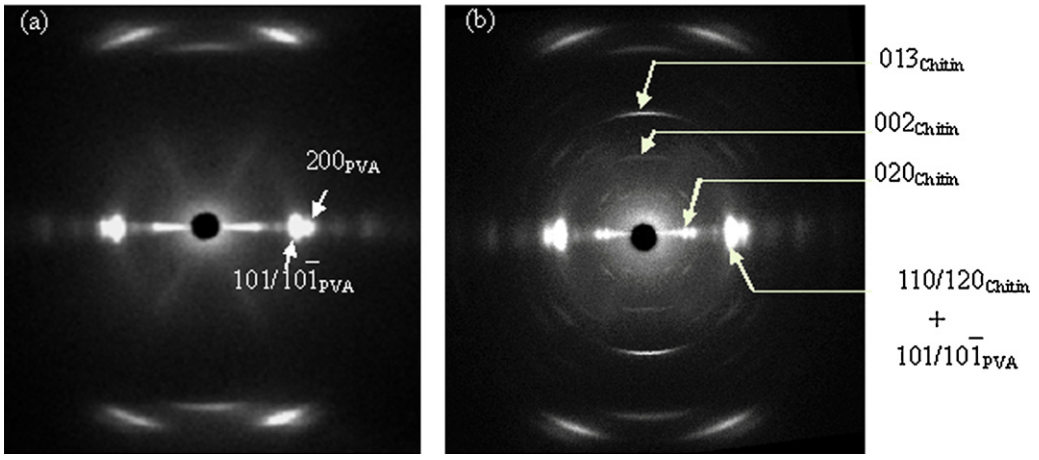

Fig. 2. WAXD images of (a) neat PVA, and (b) PVA–ChW 30% fibers.

Table 1
The maximal draw ratio (DR_{max}), fiber diameter, heat of fusion (ΔH_m), degree of crystallinity (χ_c) and melting temperature (T_m) of PVA in neat PVA and PVA–ChW fibers.

ChW content (wt%)	DR_{max}	Fiber dia. (μm)	ΔH_m (J g^{-1})	χ_c (%)	T_m (°C)
0	28	45	111	70	239
3	28	45	118	74	239
5	28	45	121	76	239
10	27	46	126	79	240
15	25	48	131	82	240
20	23	50	146	85	242
30	21	52	141	88	243

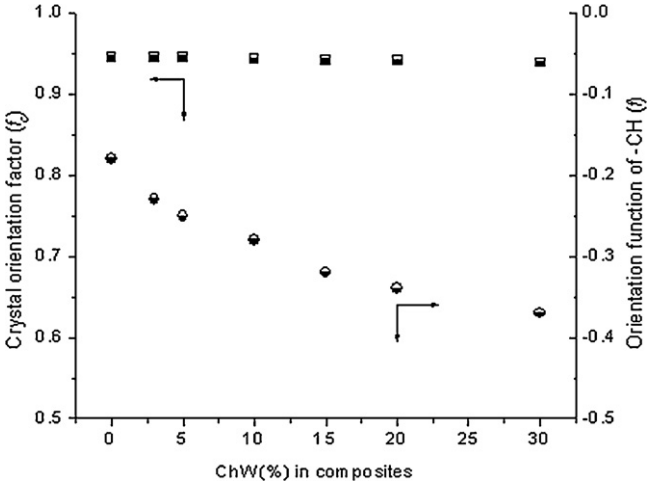

Fig. 3. Crystal orientation factor (f_c) and orientation function of –CH component (f) of PVA in neat PVA and PVA–ChW fibers.

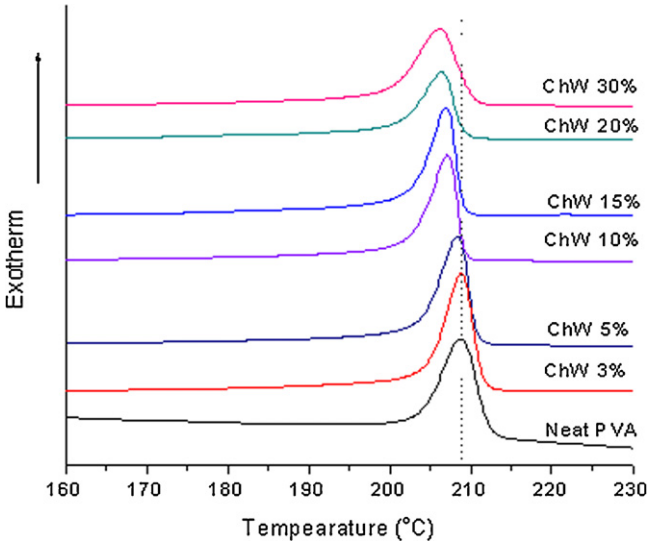

Fig. 4. DSC cooling scans of neat PVA and PVA–ChW fibers at 10 °C min^{-1} after melting to 250 °C.

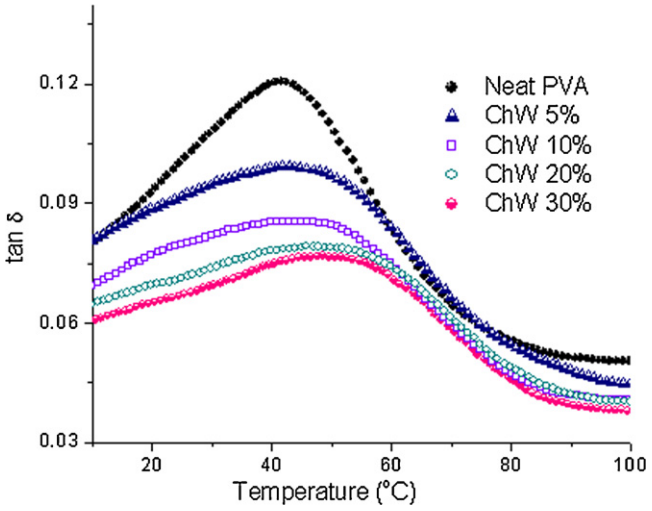

Fig. 5. Dynamic tan δ curves of neat PVA and PVA–ChW fibers.

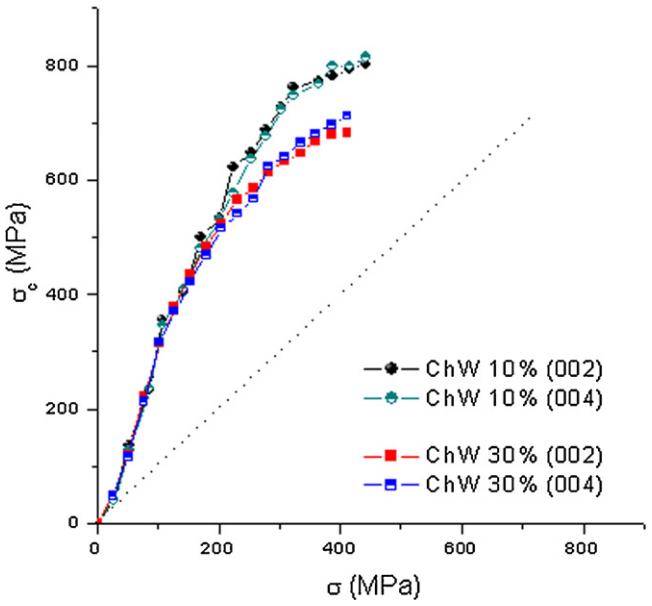

Fig. 6. The variation of the effective stress on the ChWs (σ_c) with the stress applied to PVA–ChW composite fibers (σ).

through the PVA matrix. In addition, a higher rate of stress transfer was observed, especially in the higher stress region, for the sample with lower ChW content (here 10%) compared with the sample with higher ChW content (here 30%). This can be explained by the fact that ChWs being well dispersed and adhering well to the matrix when its content is relatively lower in the composites. Conversely, the lower rate of stress transfer in case of higher ChW content might have caused by the aggregation of ChWs in composites that reduced the effectiveness in stress transfer.

3.3. Mechanical properties

Representative stress–strain curves of the neat PVA and PVA–ChW fibers are shown in Fig. 7. Compared to neat PVA, significant improvement in tensile strength, initial modulus and toughness was observed for the composite fibers. The highest tensile strength (1.88 GPa) and toughness (68 J g^{-1}) were obtained for the PVA–ChW 5% composites compared with the same of neat PVA, 1.47 GPa and 58 J g^{-1}, respectively (Table 2). It implies that the 5%

Table 2
Mechanical properties and creep rate of neat PVA and PVA–ChW fibers.

Sample	Breaking strength (GPa)	Young's modulus (GPa)	Elongation at break (%)	Toughness ($J g^{-1}$)	Loop strength (MPa)	Creep rate (% in 1000 h)
Neat PVA	1.47 ± 0.08	28 ± 3	9.7 ± 0.7	58 ± 3	155 ± 15	33
Ch W 3%	1.71 ± 0.06	36 ± 3	9.2 ± 0.2	65 ± 2	190 ± 12	22
Ch W 5%	1.88 ± 0.08	38 ± 4	9.0 ± 0.2	68 ± 3	230 ± 16	17
Ch W 10%	1.80 ± 0.11	41 ± 3	7.0 ± 0.7	48 ± 3	215 ± 14	16
Ch W 15%	1.75 ± 0.10	43 ± 4	6.2 ± 0.6	42 ± 2	195 ± 16	12
Ch W 20%	1.63 ± 0.09	46 ± 4	5.3 ± 0.7	32 ± 2	184 ± 17	11
Ch W 30%	1.50 ± 0.10	50 ± 4	4.4 ± 0.6	24 ± 4	172 ± 15	10

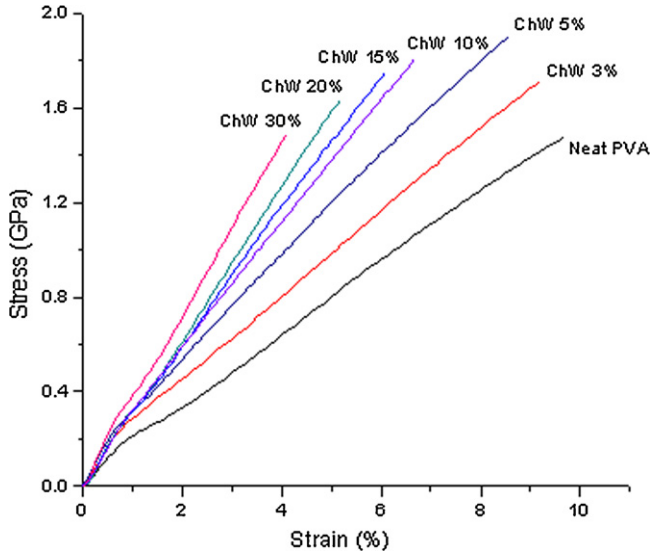

Fig. 7. Representative stress–strain curves of neat PVA and PVA–ChW fibers.

ChWs loading is the optimum loading in the context of tensile strength and toughness. Young's modulus increased almost proportionally with the ChW content. PVA–ChW 30% fiber showed Young's modulus of 50 GPa, much higher than the same of neat PVA, 28 GPa.

The thermomechanical performance of nanocomposite material is defined by the mechanical properties of the constituents and the microstructure. The morphology is characterized by parameters such as filler length and filler orientation. The influence of these parameters on Young's modulus of the composite (E_{com}) can be evaluated by a rule-of-mixtures type expression as follows (Pickering, 2008):

$$E_{com} = \eta_{LE}\eta_{OE}E_f V_f + E_m(1 - V_f) \quad (1)$$

E_m and E_f are Young's modulus for matrix and filler, respectively, V_f is the volume fraction of filler, η_{LE} is fiber length efficiency factor ($0 \le \eta_{LE} \le 1$), and η_{OE} is the orientation efficiency factor which is 1 for fully oriented fillers. Since we do not know the actual η_{LE} value, an effective filler modulus E_{eff} incorporating only the length efficiency factor of the fillers, given by $E_{eff} = \eta_{LE}E_f$, was used. Substituting the values $E_{com} = 50$ GPa, $E_m = 28$ GPa, $V_f = 0.28$ and $\eta_{OE} = 0.9$ for the PVA–ChW 30% fiber, E_{eff} of the whisker was calculated to be 118 GPa. This value is much higher than the reported modulus of α-chitin crystals (41 GPa) (Nishino et al., 1999), which indicates that the reinforcing mechanism of ChWs in our composites is not governed by the simple rule-of-mixtures. There must be some other factors that contribute to the enhanced modulus of the composites.

Neat PVA fiber was observed by optical microscopy to be dark with a series of horizontal bands generated from large interfibrillar voids during the drawing process (not shown here). The voids made the fiber opaque by inhibiting the transmission of light (Takahashi, Suzuki, Aoki, & Sakurai, 1991). Due to the existence of voids, PVA fiber had a structure with weak lateral interaction between adjacent chains. In contrast, all PVA–ChW fibers had transparent appearance in the optical microscope, indicating suppression of large void formation by the incorporation of ChWs. The significant decrease of void formation in PVA fiber after ChWs incorporation is presumed to have contributed to increasing the tensile properties. Analogous suppression of voids was also observed for PVA composites reinforced with cellulose whiskers (Uddin et al., 2011).

Due to the weak lateral interaction of chains and the existence of voids, PVA fiber usually shows a low axial compressive strength to tensile strength like Kevlar (Fawaz, Palazotto, & Wang, 1992), that limits its applications. The loop strength, a measure of a fiber's sensitivity to compression, of our neat PVA and PVA–ChW fibers were compared. The loop strength, shown in Table 2, followed a similar trend to the tensile strength, and the PVA–ChW 5% fiber showed the highest loop strength of 230 MPa that was 48% higher than that of the neat PVA (155 MPa). The configuration of the fibers during loop strength testing is shown in Fig. 8. At the bending point of the loop, the fiber undergoes severe axial stress at the outer layer and compressive stress at the inner layer. The fibrils of neat PVA fiber had relatively weak lateral connections because of the presence of voids. As a result fibers tended to split into microfibrils when tested under compression, and ultimately disintegrated. For the composite fibers the diminished voids and the interaction of PVA/ChWs led to homogeneous shearing of fibrils. Thus their loop structure was almost retained, and gave higher loop strength.

The dynamic mechanical properties of the composites have been reported to strongly depend on the filler orientation (Nielsen & Landel, 1994). Fig. 9(a) and (b) shows, respectively the storage modulus (E'), and the E' values at glassy (−100 °C) and rubbery (100 °C) regions of neat PVA and composite fibers. The significant enhancement of E' in both glassy and rubbery regions were observed after incorporating ChWs. For PVA–ChW 30% fiber, the E' at −100 °C (116 GPa) was 38% higher than that of neat PVA (84 GPa). For the same composite, the E' at 100 °C (27 GPa) was 125% higher than that of neat PVA fiber (12 GPa).

The creep strain response is considered to be an important criterion for the fibers like PVA that are used to reinforce concrete, conveyer belts and tire cords. Fig. 10 shows the creep strain behavior of PVA and PVA–ChWs fibers under a constant stress (300 MPa, more than yield stress) and at a constant temperature (120 °C). It is seen in Fig. 10 that the creep strain of PVA fiber is remarkably suppressed after incorporating ChWs into it. The creep strain rates calculated from the slope of the final linear part of the curves is shown in Table 2. The values show a very remarkable decrease with increase the ChW loading in composites. Under the constant stress the molecular chains of neat PVA fiber may slide over each other and hence the fiber elongates with time. For PVA–ChW fibers, the interaction of PVA/ChWs leading to reduction in interfibrillar voids, and increase in chain orientation and resultant increased crystallinity of PVA are assumed to immobilize the PVA chains against stress even over a long period.

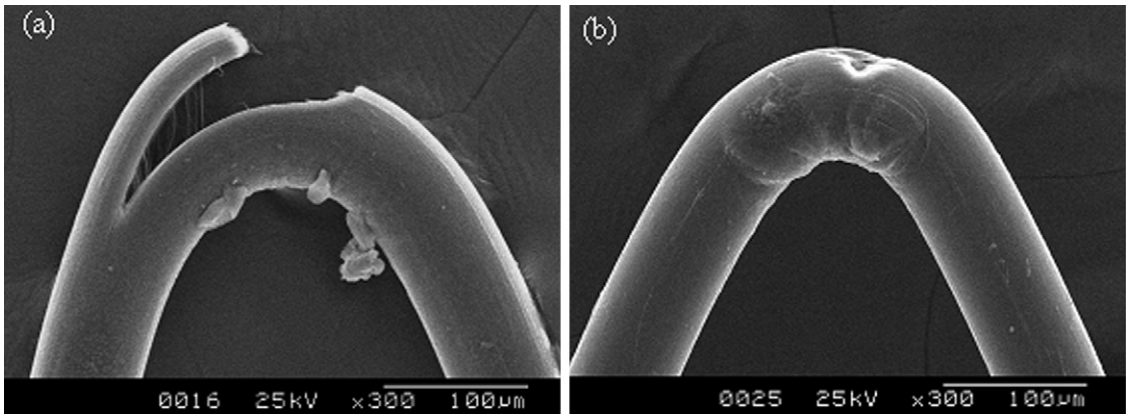

Fig. 8. The loop configuration of (a) neat PVA, and (b) PVA–ChW 5% fibers.

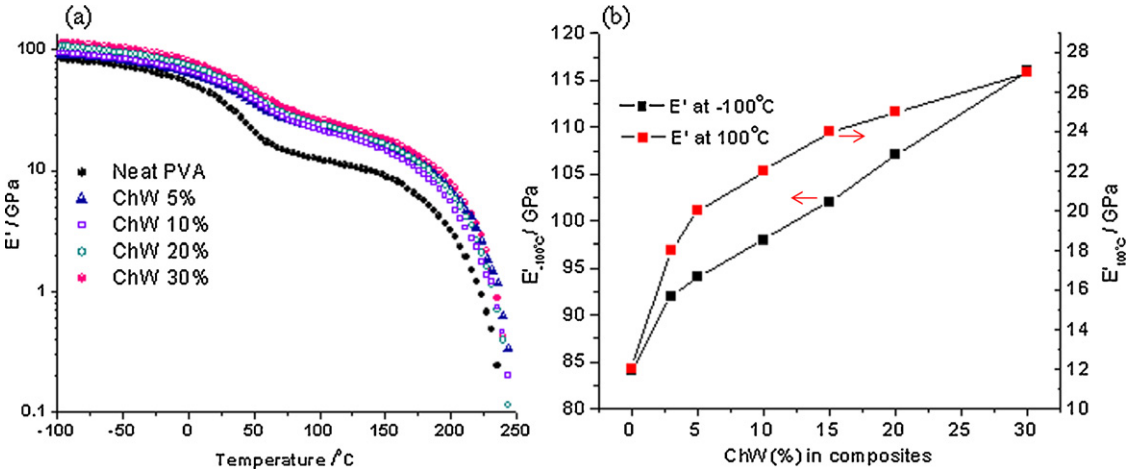

Fig. 9. (a) Storage modulus (E'), and (b) E' at −100 °C (left) and 100 °C (right) of the neat PVA and PVA–ChW fibers.

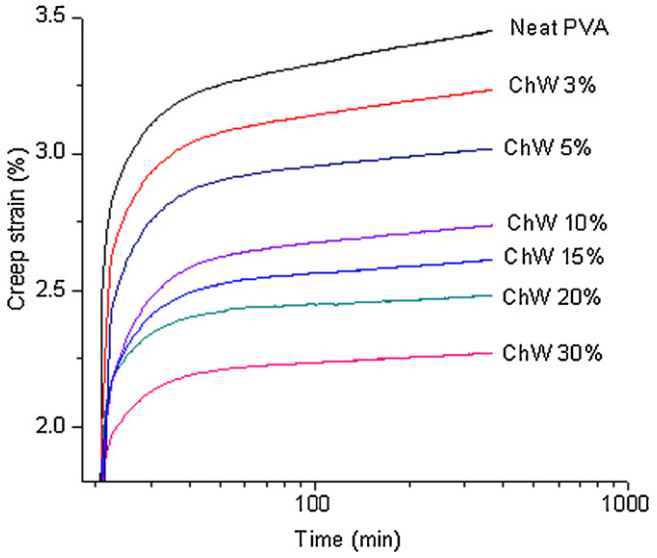

Fig. 10. Creep strain over time for neat PVA and PVA–ChW fibers at 120 °C under constant stress (300 MPa).

4. Conclusions

In this work, we prepared PVA–ChWs nanocomposite fibers where ChWs were highly oriented along the fiber axis. With increasing ChW loading in composites, the overall chain orientation and crystallinity of PVA increase, the non-isothermal crystallization temperature of PVA shifts to lower temperature, and the dynamic α-relaxation peak of PVA shifts to higher temperature, resulted from the interaction between matrix and filler. The study of stress transfer by X-ray diffraction showed effective stress transfer between matrix PVA to filler ChWs through their interface. The effect of the interfacial interaction and the stress transfer between PVA and ChWs, and higher crystallinity of PVA resulted the outstanding enhancement in the tensile-, dynamic mechanical-, and anti-creep properties of nanocomposites.

The nanocomposites prepared in this work incorporate a biobased polymer, resulting in a very strong material.

Acknowledgments

The authors are indebted to the Ministry of Education, Culture, Sports, Science and Technology of Japan for support of this work through a Grant-in-Aid for Global COE program. The authors are also thankful to Dr. Jun Araki of Shinshu University for his useful comments in preparation of chitin whiskers.

References

Azizi Samir, M. A. S., Alloin, F., & Dufresne, A. (2005). Review of recent research into cellulosic whiskers, their properties and their application in nanocomposite field. *Biomacromolecules*, *6*, 612–626.

Eichhorn, S. J., Hearle, W. S., Jaffe, M., & Mikutani, T. (2009). *Handbook of textile fibre structure*. New York: CRC Press.

Estes, G. M., Seymour, R. W., & Cooper, S. L. (1971). Infrared studies of segmented polyurethane elastomers. II. Infrared dichroism. *Macromolecules*, *4*, 452–457.

Fawaz, S. A., Palazotto, A. N., & Wang, C. S. (1992). Axial tensile and compressive properties of high-performance polymeric fibres. *Polymer*, *33*, 100–105.
Habibi, Y., Lucia, L. A., & Rojas, O. J. (2010). Cellulose nanocrystals: Chemistry, self-assembly, and applications. *Chemical Review*, *110*, 3479–3500.
Holland, B. J., & Hay, J. N. (2001). The thermal degradation of poly(vinyl alcohol). *Polymer*, *42*, 6775–6783.
Hussain, F., Hojjati, M., Okamoto, M., & Gorga, R. E. J. (2006). Polymer–matrix nanocomposites, processing, manufacturing, and application: An overview. *Journal of Composite Materials*, *40*, 1511–1575.
Junkansem, J., Rujiranavit, R., & Supaphol, P. (2006). Fabrication of α-chitin whisker-reinforced poly(vinyl alcohol) nanocomposite nanofibres by electrospinning. *Nanotechnology*, *17*, 4519.
Junkansem, J., Rujiranavit, R., Grady, B. P., & Supaphol, P. (2010). X-ray diffraction and dynamic mechanical analyses of α-chitin whisker-reinforced poly(vinyl alcohol) nanocomposite nanofibres by electrospinning. *Polymer International*, *59*, 85–91.
Kadokawa, J. I., Takegawa, A., Mine, S., & Prasad, K. (2011). Preparation of chitin nanowhiskers using an ionic liquid and their composite materials with poly(vinyl alcohol). *Carbohydrate Polymers*, *84*, 1408–1412.
Kumar, M. N. V. R., Muzzareli, R. A. A., Muzzareli, C., Sashiwa, H., & Domb, A. J. (2004). Chitosan chemistry and pharmaceutical perspectives. *Chemical Review*, *104*, 6017–6084.
Kubo, S., & Kadla, J. F. (2003). The formation of strong intermolecular interactions in immiscible blends of poly(vinyl alcohol) (PVA) and lignin. *Biomacromolecules*, *4*, 561–567.
Minke, R., & Blackwell, J. (1978). The structure of α-chitin. *Journal of Molecular Biology*, *120*, 167–181.
Nair, K. G., & Dufresne, A. (2003). Crab shell chitin whisker reinforced natural rubber nanocomposites. 1. Processing and swelling behavior. *Biomacromolecules*, *4*, 657–665.
Nielsen, L. E., & Landel, R. F. (1994). *Mechanical Properties of Polymers and Composites* (2nd edition). New York: Marcel Dekker., p. 492.
Nishino, T., Matsui, R., & Nakamae, K. (1999). Elastic modulus of the crystalline regions of chitin and chitosan. *Journal of Polymer Science: Part B: Polymer Physics*, *37*, 1191–1196.
Pickering, K. L. (2008). *Properties and performance of natural-fibre composites*. New York: CRC press.
Quan, H., Li, Z. M., Yang, M. B., & Huang, R. (2005). On transcrystallinity in semi-crystalline polymer composites. *Composite Science & Technology*, *65*, 999–1021.
Read, B. E., & Stein, R. S. (1968). Polarized infrared studies of amorphous orientation in polyethylene and some ethylene copolymers. *Macromolecules*, *1*, 116–126.
Rusli, R., Shanmuganathan, K., Rowan, S. J., Weder, C., & Eichhorn, S. J. (2010). Stress-transfer in anisotropic and environmentally adaptive cellulose whisker nanocomposites. *Biomacromolecules*, *11*, 762–768.
Sakurada, I., Nukushina, Y., & Ito, Y. (1962). Experimental determination of the elastic modulus of crystalline regions in oriented polymers. *Journal of Polymer Science*, *57*, 651–660.
Sriuayo, J., Supaphol, P., Blackwell, J., & Rujiranavit, R. (2005). Preparation and characterization of α-chitin whisker-reinforced poly(vinyl alcohol) nanocomposite films with or without heat treatment. *Polymer*, *46*, 5637–5644.
Sun, W., Chen, H., Luo, X., & Qian, H. (2001). The effect of hybrid fibres and expansive agent on the shrinkage and permeability of high-performance concrete. *Cement & Concrete Research*, *31*, 595–601.
Takahashi, T., Suzuki, K., Aoki, T., & Sakurai, K. (1991). Banded structure of gel-drawn poly(vinyl alcohol) fibres. *Journal of Macromolecular Science & Physics*, *30*, 101–108.
Uddin, A. J., Araki, J., & Gotoh, Y. (2011). Extremely oriented tunicin whiskers in poly(vinyl alcohol) nanocomposites. *Polymer International*, *60*, 1230–1239.
Uddin, A. J., Mashima, Y., Ohkoshi, Y., Gotoh, Y., Nagura, M., Sakamoto, A., et al. (2006). Drawing behavior and characteristics of laser-drawn polypropylene fibres. *Journal of Polymer Science: Part B: Polymer Physics*, *44*, 398–408.
Wang, Z., Ciselli, P., & Peijs, T. (2007). The extraordinary reinforcing efficiency of single-walled carbon nanotubes in oriented poly(vinyl alcohol) tapes. *Nanotechnology*, *18*, 455709.
Zheng, Z., & Feldman, D. (1995). Synthetic fibre-reinforced concrete. *Progress in Polymer Science*, *20*, 185–210.